Altered dynein-dependent transport in piRNA pathway mutants

Caryn Navarro[a,1], Simon Bullock[b], and Ruth Lehmann[a,2]

[a]Developmental Genetics Program, the Skirball Institute, the Kimmel Center for Biology and Medicine, the Howard Hughes Medical Institute and the Department of Cell Biology, New York University School of Medicine, 540 First Avenue, New York, NY 10016; and [b]Medical Research Council Laboratory of Molecular Biology, Hills Road, Cambridge CB2 0QH, United Kingdom

Contributed by Ruth Lehmann, April 10, 2009 (sent for review August 5, 2008)

Maintenance of genome integrity in germ cells is crucial for the success of future generations. In *Drosophila*, and mammals, transposable element activity in the germline can cause DNA breakage and sterility. Recent studies have shown that proteins involved in piRNA (PIWI-interacting RNA) biogenesis are necessary for retrotransposon silencing in the *Drosophila* germline. Females mutant for genes in the piRNA biogenesis pathway produce eggs with patterning defects that result from Chk-2 (checkpoint kinase-2) DNA damage checkpoint activation. Here we show that large ribonucleoprotein aggregates form in response to DNA damage checkpoint activation in egg chambers of females defective in piRNA biogenesis. Aggregate formation is specific to piRNA biogenesis mutants, as other mutations that activate the same Chk-2-dependent checkpoint do not cause aggregate formation. These aggregates contain components of the dynein motor machinery, retrotransposon RNA, and protein and axial patterning RNAs. Disruption of the aggregates by colcemid treatment leads to increased retrotransposon RNA levels, indicating that these structures may be the destination of retrotransposon RNA transport and may be degradation or sequestration sites. We propose that aggregate formation is a cellular response to protect germ cells from DNA damage caused by elevated retrotransposon expression.

DNA damage | *Drosophila* germline | retrotransposon | RNA transport

The *Drosophila melanogaster* embryonic axes are established during oogenesis through the differential localization of RNA molecules (1). RNAs and proteins are initially synthesized in the nurse cells, sister cells of the oocyte that are connected to the oocyte by large cytoplasmic bridges. Subsequently, these molecules are transported along a microtubule network into the oocyte in a process dependent on the dynein motor complex (2). Within the oocyte, RNAs necessary for the establishment of the anterior/posterior (A/P) and dorsal/ventral (D/V) embryonic axes such as *bicoid* (*bcd*), *oskar* (*osk*), and *gurken* (*grk*), are differentially localized to the anterior, posterior, and dorsoanterior regions of the egg, respectively (1). Failure to correctly localize these RNA molecules to and within the oocyte causes axial patterning defects in the resulting embryos.

In addition to embryonic patterning molecules, retrotransposon RNA also localizes to and within the oocyte (3, 4). One of the best studied of these elements is the non-LTR (long terminal repeat) retrotransposon, I factor, the *Drosophila* counterpart of the mammalian LINE-1 element. I factor RNA localizes, in a dynein-dependent manner, within the *Drosophila* oocyte in a pattern similar to *grk* RNA (4). It has been proposed that I factor transposition causes defects in *grk* RNA localization because of a competition between *grk* and I factor RNA for the same localization machinery (4).

Female flies with mutations in several genes in the piRNA biogenesis pathway such as *spindle E* (*spnE*), *aubergine* (*aub*), and *armitage* (*armi*) lay eggs with D/V patterning defects, because of cytoskeletal changes that result in the mislocalization of *grk* RNA within the egg chamber (5–7). These defects have been linked to the Chk-2 DNA damage checkpoint that may be activated by increased retrotransposon RNA levels in mutants defective in piRNA biogenesis (8, 9). How checkpoint activation causes changes in the cytoskeletal network is currently unknown. One possibility is that checkpoint activation directly modifies the RNA transport machinery.

Here we show that large aggregates of the dynein motor machinery form in nurse cells and oocytes defective in piRNA biogenesis. These transport aggregates carry patterning RNAs and retrotransposon RNAs and proteins. Their assembly requires the microtubule network and occurs in response to Chk-2 checkpoint activation. Our findings suggest that aggregate formation is a specific cellular response to DNA damage and elevated retrotransposon RNA levels resulting from defective piRNA biogenesis. We propose that the dynein motor machinery transports retrotransposon RNA to and accumulates at retrotransposon degradation sites in the absence of piRNA biogenesis.

Results

The Dynein Motor Machinery Forms Cytoplasmic Aggregates in piRNA Biogenesis Mutants. In most piRNA pathway mutant egg chambers Chk-2 DNA damage checkpoint activation results in defects in microtubule network polarization and axial patterning (8–10). To determine how checkpoint activation may affect the microtubule network, we analyzed the distribution of the dynein motor complex, which controls RNA transport into and within the oocyte, in piRNA pathway mutant egg chambers. In egg chambers mutant for *spnE*, *aub*, *armi*, *maelstrom* (*mael*), and *vasa* (*vas*) we observed large aggregates of Dynein Heavy Chain (DHC), Dynamitin (Dmn), Egalitarian (Egl) and Bicaudal-D (BicD) (Fig. 1 *A–E″*, for BicD in *spnE* also see refs. 11, 12; for BicD and Egl in *vas* also see ref. 13; supporting information (SI) Fig. S1, Table S1). These dynein aggregates were found between stages 4 and 9 of oogenesis within the nurse cell and oocyte cytoplasm (Fig. 1 *F–G′*).

To further characterize these dynein aggregates we analyzed the localization of proteins with functions in RNA localization, translational regulation, and RNAi, such as processing body, stress granule, and aggresome components in *spnE*, *aub*, *armi*, and *vas* mutant backgrounds. We found that most of these proteins do not colocalize with the dynein aggregates (Table S2). Relative to the general cytoplasmic staining, a small enrichment of Orb (oo18 RNA binding protein), Tudor, Cup, Me31B, and Dcp-1 proteins was detected within the aggregates, and a small amount of Exuperantia (Exu) was found in the oocyte aggregate;

Author contributions: C.N. and R.L. designed research; C.N. performed research; C.N. and S.B. contributed new reagents/analytic tools; C.N. and R.L. analyzed data; and C.N. and R.L. wrote the paper.

The authors declare no conflict of interest.

Freely available online through the PNAS open access option.

[1]Present address: Department of Medicine/Genetics Program, Boston University School of Medicine, 72 E. Concord Street, L320, Boston, MA 02118.

[2]To whom correspondence should be addressed. E-mail: lehmann@saturn.med.nyu.edu.

This article contains supporting information online at www.pnas.org/cgi/content/full/0903837106/DCSupplemental.

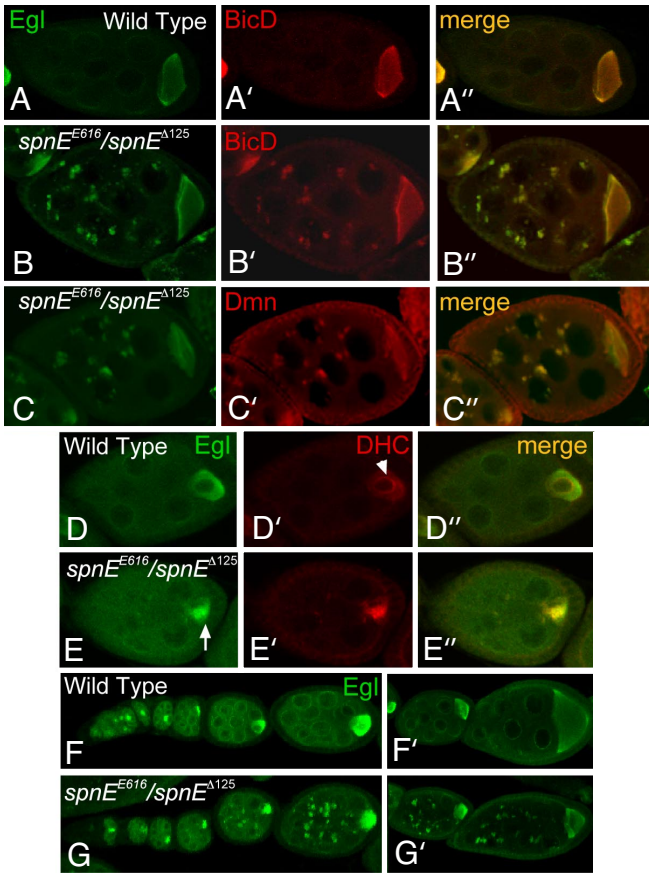

Fig. 1. The dynein localization machinery forms aggregates in piRNA pathway mutant egg chambers. (*A–C′′*) Stage 8 egg chambers stained with (*A*, *B*, and *C*) anti-Egl (green), (*A′* and *B′*) anti-BicD (red), (*C′*) anti-Dmn (red), and (*A′′*, *B′′*, and *C′′*) merge (yellow). (*A–A′′*) Wild-type egg chambers, Egl and BicD, colocalize within the oocyte (*A′′*, yellow). (*B–B′′*) $spnE^{616}/spnE^{\Delta 125}$egg chambers. Aggregates of Egl and BicD form in the nurse cells of these mutant egg chambers. The aggregates of Egl and BicD colocalize (*B′′*, yellow). (*C–C′′*) Aggregates of Dmn colocalize with Egl aggregates in $spnE^{616}/spnE^{\Delta 125}$ mutant egg chambers (*C′′*, yellow). (*D–E′′*) Egl and dynein form an aggregate at stages 5 and 6 in *spnE* mutant oocytes. Egl (green), DHC (red), merge (yellow). (*D–D′′*) In wild type, Egl and DHC localize to the oocyte with Egl localizing to a more posterior region of the oocyte and DHC localizing around the oocyte nucleus (arrowhead). (*E–E′′*) In $spnE^{616}/spnE^{\Delta 125}$ mutant egg chambers Egl and DHC localize to a tight focus, along the side or at the posterior of the oocyte (arrow). (*F–G′*) Localization machinery clustering begins at stage 4 of oogenesis and continues past stage 9. (*F* and *F′*) Wild-type ovariole (string of developing egg chambers) stained with anti-Egl (green). (*G* and *G′*) $spnE^{616}/spnE^{\Delta 125}$ ovariole stained with anti-Egl (green). (*F′* and *G′*) Later-stage egg chambers from same ovariole as in *F* and *G*, respectively.

however, the degree of enrichment of these proteins was considerably less than that of Egl, BicD, and DHC (Table S2). The prominent and specific enrichment of Egl, BicD, and DHC within these aggregates suggests that loss of *spnE*, *aub*, *armi*, *mael*, and *vas* activity specifically interferes with the normal distribution of the dynein transport machinery.

Dynein Aggregation Requires an Intact Microtubule Network. Dynein-based movement relies on the microtubule network for directional molecular transport (14). We therefore tested whether the formation or stability of the aggregates is dependent on an intact microtubule network. We depolymerized the microtubule network in ovaries from *spnE*, *armi*, or *vas* mutant flies by feeding them colcemid and assayed for aggregates by staining the egg chambers with α-Egl antibody (Fig. 2). As previously

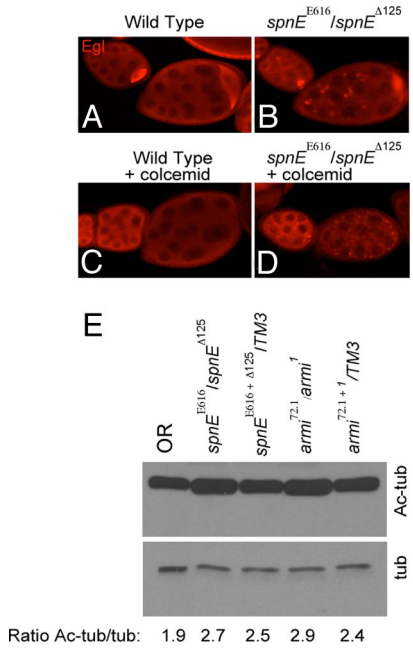

Fig. 2. Dynein aggregation depends on the microtubule network and may stabilize the microtubule network. (*A–D*) Dynein localization machinery clusters are not present after microtubule depolymerization. (*A–D*) Anti-Egl stained egg chambers (red). (*A*) Wild-type egg chambers showing strong Egl accumulation within the oocyte. (*B*) $spnE^{\Delta 125}/spnE^{E616}$ egg chambers with Egl aggregates in the nurse cells. (*C*) Wild-type egg chambers after colcemid treatment. Notice the lack of Egl accumulation within the oocyte. (*D*) $spnE^{\Delta 125}/spnE^{E616}$ egg chambers after colcemid treatment. Smaller Egl aggregates are found throughout the egg chamber. (*E*) Acetylated tubulin protein levels are elevated in *spnE* and *armi* mutant ovarian extracts. By Western blotting the ratio of acetylated tubulin to total cellular tubulin is increased in *spnE* and *armi* mutant egg chambers. Western blots were repeated 4 times for *spnE* and 3 times for *armi* with 4 independent samples for *spnE* and 3 independent samples for *armi*.

reported, after 16–24 h of colcemid treatment microtubule-based transport to and within the oocyte, as judged by Egl staining, was decreased in otherwise wild-type egg chambers (Fig. 2*C*) (15). In the colcemid-treated mutant egg chambers, smaller, and in some cases no Egl clusters were found within the nurse cells, compared to control chambers that had not been exposed to the drug (Fig. 2 *A–D*, Fig. S2). These smaller clusters suggested that the microtubule network was not completely depolymerized in the mutants after drug treatment. Indeed, we found that the level of acetylated tubulin, a modification of α-tubulin characteristic of stable microtubules (16), was increased in extracts from piRNA pathway mutant ovaries (Fig. 2*E*). These results suggest that an intact microtubule network is required for the formation or stability of the enlarged dynein aggregates and that mutations in piRNA pathway components may cause a more stable microtubule network to form.

Dynein Aggregates Contain *bicoid* and *gurken* RNAs. The microtubule network and the dynein motor machinery transport RNAs encoding patterning molecules from the nurse cells to the oocyte and also within the oocyte. To determine whether the large dynein aggregates in piRNA biogenesis mutants contain RNA we analyzed the distribution *bcd*, *osk*, *fs (1)K10*, and *grk* RNA. *bcd* RNA colocalized with Egl in aggregates in nurse cells of *spnE*, *armi*, *aub*, and *vas* mutant egg chambers (Fig. 3 *A–C″*, Fig. S3, for *spnE* see also ref. 11), while *grk*, *osk*, and *fs (1)K10* mRNAs were found in the large Egl-positive aggregate within the oocyte of these mutants (Fig. 3 *D* and *E*, Fig. S3, Table S3).

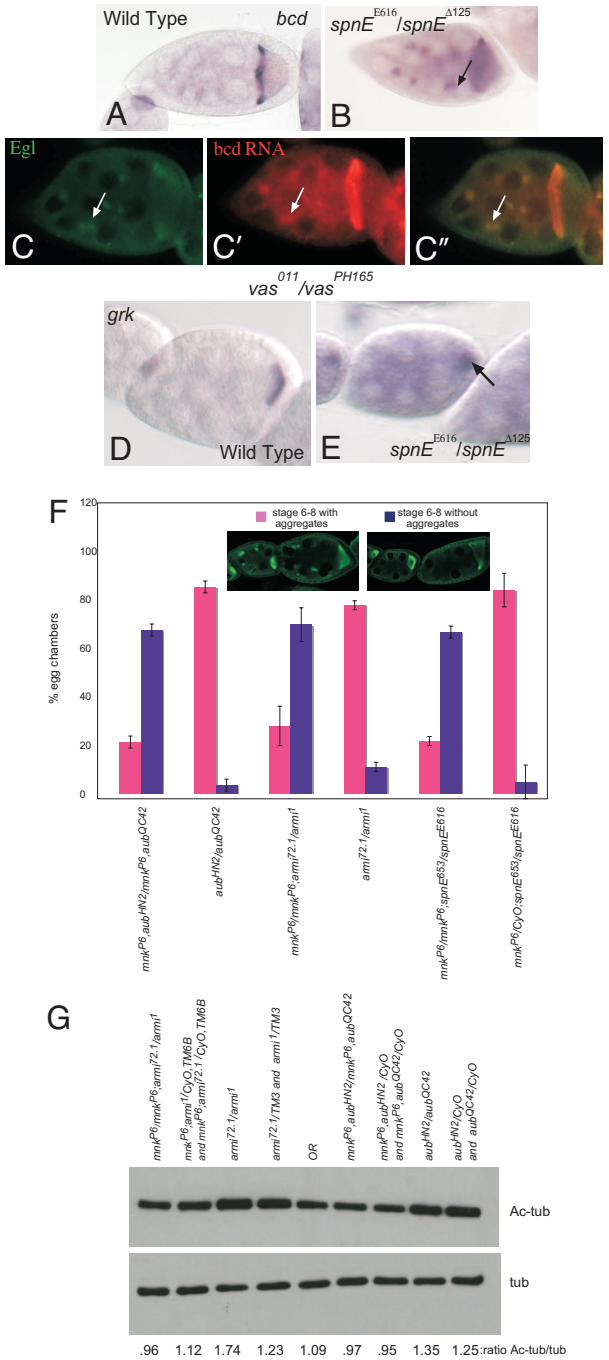

Fig. 3. The dynein aggregates are RNP particles and result from Chk-2 checkpoint activation. (*A* and *B*) Stage 9 egg chambers. *bcd* RNA localization in *A* wild type, in *B* $spnE^{\Delta 125}/spnE^{E616}$ mutant egg chambers. *bcd* RNA forms aggregates in the nurse cells of the mutant egg chambers (arrows). (*C*–*C*′′) *bcd* RNA colocalizes with Egl protein in the nurse cell aggregates in vas^{011}/vas^{PH165} mutant egg chambers. (*C*) vas^{011}/vas^{PH165} mutant egg chamber showing aggregates of Egl protein. (*C*′) vas^{011}/vas^{PH165} mutant egg chamber showing aggregates of *bcd* RNA. (*C*′′) merge of *C* and *C*′. (*D* and *E*) *grk* RNA localization at stage 5 of oogenesis. (*D*) Wild-type *grk* RNA localization. (*E*) *grk* RNA localization in $spnE^{\Delta 125}/spnE^{E616}$. *grk* RNA forms an aggregate along the side of or at the posterior of the oocyte in the mutant egg chambers. Arrows point to RNA aggregates. (*F*) Mutations in the Chk-2 (*mnk*) DNA damage checkpoint suppress the dynein aggregation phenotype of *aub*, *armi*, and *spnE* mutant egg chambers. Representative images are of *aub* mutant egg chambers stained with α-Egl antibody (green) to visualize the aggregates. Dissections were preformed on 2 separate days and the average results from these 2 experiments are shown in the figure. (*G*) The elevated levels of acetylated tubulin in piRNA pathway mutant ovaries are returned to wild type in the double mutant *mnk*;*piRNA* pathway mutant ovaries.

gcl RNA, which in wild type is more evenly distributed throughout nurse cells and oocytes (P. Rangan and R.L. personal communication), was found neither in the nurse cell nor in the oocyte aggregates (Table S3), suggesting that actively transported RNAs preferentially accumulate in dynein aggregates. We conclude that dynein aggregates represent true RNP particles.

If RNAs required for oocyte and embryonic axis formation are indeed sequestered into large dynein aggregates in piRNA biogenesis mutants, these RNP aggregates may prevent normal RNA transport and cause the patterning defects observed in these mutants. Indeed, we found that reduction of the motor components BicD or Dhc partially suppressed the D/V axial patterning defects in eggs laid by *spnE* or *aub* mutant mothers (Table 1). Therefore, dynein-mediated RNA transport into aggregates contributes to the axial patterning defects in piRNA pathway mutant flies.

Dynein Aggregation Is a Consequence of Chk-2 DNA Damage Checkpoint Activation. Microtubule network changes and axial patterning defects seen in the piRNA pathway mutant eggs are the result of Chk-2 DNA damage checkpoint activation (8–10). We therefore asked whether Chk-2 checkpoint activation causes dynein aggregation in piRNA biogenesis mutants. We analyzed dynein aggregates in flies doubly mutant for the Chk-2 checkpoint gene, *mnk* and piRNA pathway genes *aub*, *armi*, and *spnE*. We found that the number of egg chambers with large dynein aggregates was reduced in doubly mutant egg chambers compared to single mutant ovaries (Fig. 3*F*). Additionally we tested whether the elevated levels of acetylated tubulin in the piRNA pathway mutant egg chambers also resulted from checkpoint activation. We found that the level of acetylated tubulin in flies double mutant for the Chk-2 checkpoint gene and the piRNA pathway genes was reduced to wild-type levels (Fig. 3*G*). These results suggest that Chk-2 checkpoint activation in piRNA biogenesis mutants leads to dynein machinery aggregation and elevated levels of acetylated tubulin.

We next asked whether checkpoint activation in general leads to dynein aggregates or whether these particles are specific to the piRNA pathway mutants. Females with mutations in the double strand break repair enzymes *spn-A* (Rad-51), *spn-B* (DMC-1), and *spn-D* (Rad51-C like) produce ovaries with RNA localization and eggshell patterning defects very similar to the piRNA pathway mutants (6, 17, 18). Furthermore, mutations in members of both pathways activate the Chk-2 DNA damage checkpoint (9, 10, 19). In contrast to mutants defective in piRNA biogenesis, we failed to detect any dynein aggregates in the nurse cells of *spnA*, *spnB*, or *spnA*,*B* double mutants (Table S1). We conclude that dynein aggregate formation is a specific response to DNA damage checkpoint activation because of defective piRNA biogenesis.

I Factor RNA Localizes to the Dynein Aggregates. The non-LTR retrotransposon, I factor RNA, uses the same dynein-based microtubule motor machinery as *fs (1)K10* and *grk* RNA for its localization to and within the oocyte (4). Along with several other retrotransposons such as Het-A and TART, I factor RNA levels are increased in piRNA pathway mutant egg chambers (20). We therefore tested if I factor, Het-A, or TART RNAs were also found associated with the enlarged dynein aggregates. By in situ hybridization we were unable to detect these RNAs in the nurse cell aggregates. However, we did detect these RNAs in the oocyte aggregate (Fig. 4 *A*–*B*′, Table S3) and using an antibody to the ORF-1 I factor protein we found I factor protein enriched in the nurse cell aggregates of *aub* and *armi* mutant egg chambers (Fig. S4).

Because I factor protein accumulated in mutant nurse cell aggregates we reasoned that I factor RNA may be present in the aggregates but below detection level. To directly observe RNA

Table 1. Suppression of piRNA biogenesis mutant patterning defects by dynein motor complex members

Genotype	Wild type (%)	Fused (%)	No, collapsed (%)	*n*
$spnE^{E616}$ or $^{\Delta 125}$/*TM3*	100	0	0	100
$spnE^{E616}/spnE^{\Delta 125}$	0	44 ± 11	56 ± 11	183
+/*CyO*;$spnE^{E616}/spnE^{\Delta 125}$	1.75 ± 1.5	23.2 ± 11.9	75 ± 12.3	794
$BicD^{R6}$/+;$spnE^{E616}/spnE^{\Delta 125}$	17 ± 4.9	44 ± 5.1	38.8 ± 9.4	1329
$BicD^{R6}$/+;$spnE^{E616}$/+ or $spnE^{\Delta 125}$/TM3	99.7 ± 0.47	0	0.33 ± 0.47	286
$BicD^{R6}$/+;+/TM3	100	0	0	201
+/*CyO*;$spnE^{E616}$/+ or $spnE^{\Delta 125}$/TM3	100	0	0	257
+/*CyO*;+/TM3	99 ± 0.8	0	1.1 ± 0.82	283
aub^{HN2} or $^{QC42/CyO}$	100	0	0	100
aub^{HN2}/aub^{QC42}	10.1 ± 6.7	35.4 ± 10.9	54.6 ± 8.3	489
aub^{HN2}/aub^{QC42};+/*TM6*	0	13.3 ± 3.3	86.3 ± 3.1	75
aub^{HN2}/aub^{QC42};*DHC*/+	19 ± 1.2	46.3 ± 8	36.7 ± 6.9	439
aub^{HN2}/*CyO* or aub^{QC42}/+;*DHC*/+	100	0	0	100
+/*CyO*;*DHC*/+	100	0	0	100
aub^{HN2}/*CyO* or aub^{QC42};+/*TM6*	100	0	0	100
+/*CyO*;+/TM6	100	0	0	100

Mutations in members of the dynein motor complex suppress the D/V patterning defects in piRNA pathway mutant eggs. Eggs were collected on apple juice agar plates overnight and sorted into categories on the basis of their respiratory appendage phenotype, which is an indication of D/V patterning. The percentage of eggs of each class represents the average of 3 separate collections. Note that there is a dramatic change in the phenotype between aub^{HN2}/aub^{QC42} *mutants and* aub^{HN2}/aub^{QC42};+/*TM6*. We cannot rule out the possibility that something on the TM6 chromosome enhances the *aub* phenotype. However, when comparing each of these genotypes to aub^{HN2}/aub^{QC42};*DHC*/+ we see a suppression of the phenotype although it is less dramatic when comparing aub^{HN2}/aub^{QC42} *to* aub^{HN2}/aub^{QC42};*DHC*/+. Wild type, two separate dorsal appendages; fused, fused dorsal appendages; no, collapsed, no dorsal appendages or collapsed eggs.

transport toward the dynein aggregates, we injected I factor RNA into mutant nurse cells. When we injected highly concentrated fluorescently labeled I factor RNA into *vas* mutant nurse cell cytoplasm, the transcripts accumulated within the dynein aggregate, whereas the control nonlocalizing RNA, *Krueppel*, did not localize to a specific region within the nurse cells (Fig. 4*C*, Movie S1–S4). Therefore, while endogenous I factor RNA levels appear below detection, the injected retrotransposon RNA can be actively incorporated into the nurse cell aggregates. Together these data imply that endogenous I factor RNA is transported to and translated in the dynein aggregates.

Dynein Aggregates May Be Sites of Retrotransposon RNA Degradation. Aggresomes, processing bodies and stress granules, large cytoplasmic bodies found in many cell types, also require an intact microtubule network and the dynein motor machinery for their formation and/or stability (21–23). These bodies have been proposed to be sites of cellular or viral RNA and protein storage or degradation (24, 25). To test if the dynein aggregates we observe regulate intracellular retrotransposon RNA levels, we assessed the consequences of inhibiting them by depolymerizing the microtubule network in the piRNA pathway mutant egg chambers. In these experiments, the relative change in retrotransposon RNA levels was compared between piRNA pathway mutant ovaries treated with colcemid to ovaries of the same genotype that had not been treated with colcemid, as measured by quantitative RT-PCR (see Fig. 4 legend for more details). After microtubule depolymerization, egg chambers from *armi* and *aub* mutant mothers had elevated RNA levels of the non-LTR retrotransposon, Het-A, but not of the housekeeping gene *aldehyde dehydrogenase* or the patterning RNA *bcd* when compared to mutant egg chambers where the microtubule network was intact (Fig. 4*D*, *bcd* not shown). Degradation of retrotransposon RNA in dynein aggregates may explain why we failed to detect retrotransposon RNA in mutant nurse cell aggregates. Because the level of *bcd* RNA did not change upon disruption of the aggregates, the aggregates found in the *armi* and *aub* mutant ovaries may specifically degrade retrotransposon RNA in a piRNA independent manner.

In contrast to *armi* and *aub* mutant egg chambers, when we examined retrotransposon RNA levels after microtubule depolymerization in *spnE* mutant egg chambers we found a decrease in retrotransposon RNA levels (Fig. 4*D*). In support of these data, reducing the amount of the dynein motor component BicD in the *spnE* mutant background caused a decrease in the RNA levels of the Het-A retrotransposon and the LTR retrotransposon mdg-1 (Fig. S5). Differences have previously been seen between *spnE* mutants compared with *armi* and *aub* mutants (9, 10). For example, the D/V patterning defects of *armi* and *aub* mutant eggs are suppressed by mutations in the Chk-2 (*mnk*) DNA damage checkpoint kinase, whereas the *spnE* patterning defects are not (9, 10). This suggests that *spnE* may have additional functions independent of piRNA processing. These additional functions of *spnE* may target RNA stability and translation through regulation of the *Drosophila* CPEB, Orb. In *spnE* mutant ovaries Orb levels are significantly decreased, whereas, in *aub* and *armi* mutants, Orb levels remain close to wild type (ref. 26; C.N. and R.L. unpublished data). Indeed, we were able to detect I factor protein within the aggregates in *armi* and *aub* but not *spnE* mutant egg chambers. This raises the possibility that SpnE, through its effect on Orb levels, may directly affect translation of RNAs encoding patterning molecules and retrotransposon proteins in dynein aggregates independently of its role in piRNA processing.

Discussion

Here we show that mutations in piRNA pathway members cause aggregation of the dynein-mediated microtubule motor complex during *Drosophila* oogenesis. Aggregation is dependent on the activation of the Chk-2 DNA damage checkpoint and is specific to piRNA pathway mutants. Our results suggest that the dynein aggregates form in response to high levels of retrotransposon RNA in piRNA mutant ovaries. The aggregates may accumulate at sites of retrotransposon sequestration or degradation and may prevent retrotransposon RNA from entering the oocyte nucleus, thus protecting the germline from DNA damage. We propose that this response also occurs in wild-type ovaries, although less robustly because of relatively low retrotransposon load compared to piRNA biogenesis mutants.

The dynein aggregates we observe may represent enlarged RNA transport particles derived from ribonucleoprotein (RNP) particles that normally transport RNA molecules from the nurse

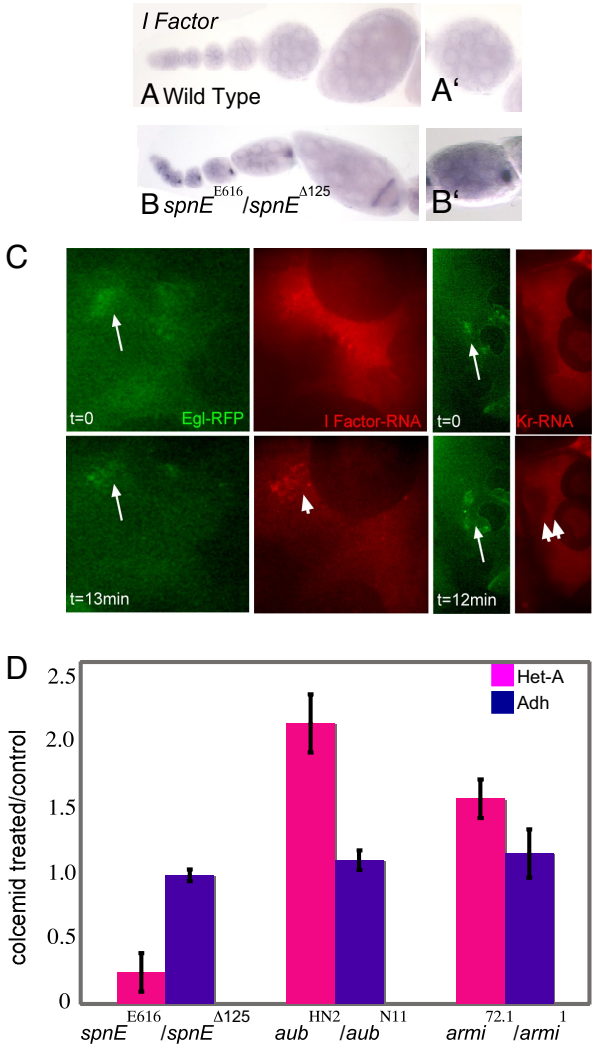

Fig. 4. The dynein aggregates accumulate I factor RNA and may be sites of retrotransposon degradation. (*A*–*B*′) I factor RNA localization during oogenesis. (*A* and *A*′) Wild-type ovariole showing no detectable localization of I factor throughout oogenesis. (*B* and *B*′) $spnE^{\Delta 125}/spnE^{E616}$ mutant ovariole showing I factor RNA expression and localization throughout oogenesis. (*B*′) An aggregate of I factor RNA is found within the oocyte of $spnE^{\Delta 125}/spnE^{E616}$ mutant egg chambers. (*C*) Exogenously injected I factor RNA is transported to the nurse cell aggregates in vas^{011}/vas^{PH165} mutant egg chambers. At time 0 ($t = 0$) I factor RNA is found uniformly distributed at the site of injection. After 13 min ($t = 13$ min), a large accumulation of I factor RNA is found associated with the Egl aggregate. In contrast, the nonlocalizing RNA Kruppel (Kr) is found uniformly distributed at all time points. The 2 different Kr panels are 2 different focal planes because of drift during filming. While filming we did focus up and down and never saw Kr localizing to the Egl aggregates. I factor RNA (red), Egl-RFP protein (green), Kr RNA (red). Arrow points to Egl aggregate; arrowhead points to injected I factor RNA aggregate; double arrowhead points to where an Egl aggregate is in the Kr RNA injected egg chamber. (*D*) Retrotransposon RNA levels decrease after microtubule depolymerization in $spnE^{\Delta 125}/spnE^{E616}$ mutant egg chambers and increase in aub^{HN2}/aub^{N11} and $armi^{72.1}/armi^{1}$ mutant egg chambers. The RNA levels of the LTR retrotransposon Het-A, and the housekeeping gene *Adh*, were measured by quantitative RT-PCR. The change in relative expression was calculated as the value of $2^{-\Delta\Delta Ct}$, where, for example, $\Delta\Delta Ct_{(colcemid\ treated)} = \Delta Ct\ (spnE^{\Delta 125}/spnE^{E616})_{colcemid\ treated} - \Delta Ct(spnE^{\Delta 125}/Balancer\ and\ spnE^{E616}/Balancer\ combined)_{colcemid\ treated}$ and $\Delta\Delta Ct_{(control\ untreated)} = \Delta Ct(spnE^{\Delta 125}/spnE^{E616})_{control\ untreated} - \Delta Ct(spnE^{\Delta 125}/Balancer\ and\ spnE^{E616}/Balancer\ combined)_{control\ untreated}$. The number shown on the graph is the ratio of the change in relative expression of colcemid-treated samples compared to the change in relative expression of untreated samples of the same genotype, $2^{-\Delta\Delta Ct(colcemid)}/2^{-\Delta\Delta Ct(untreated\ control)}$. Ct values are the threshold cycle, or the number of cycles required for the fluorescent signal to cross the threshold, thus exceeding background levels. All Ct values are normalized to the housekeeping RNA, rp49 = ΔCt.

cells to and within the oocyte. In general, DNA damage checkpoint activation causes changes in microtubule network polarity in the oocyte (9). While accumulation of patterning RNA into large dynein aggregates in the oocyte may be a consequence of such changes in microtubule network polarity, nurse cell aggregates are only observed in response to checkpoint activation in piRNA biogenesis mutants. We observe that *bcd* RNA, which localizes to the oocyte beginning at stage 4 of oogenesis, is present in nurse cell aggregates, while *grk*, *osk*, and *fs (1)K10* mRNAs, which are transported to the oocyte during early oogenesis (germarial region 2b for *osk* and *grk*) and before we detect nurse cell aggregates, are only found in oocyte aggregates. One possibility is that nurse cell aggregates form as retrotransposon levels increase, and that early transported RNAs such as *grk*, *osk*, and *fs (1)K10* mRNAs reach the oocyte before these nurse cell aggregates form.

Because axial patterning and cytoskeletal polarity within the *Drosophila* oocyte require the correct spatial and temporal localization of patterning mRNAs (27), changes in dynein motor activity could disrupt the timing and/or localization of these RNAs leading to the patterning defects seen in piRNA pathway mutant eggs. Alternatively, BicD and DHC activity could play a more direct role in modifying the cytoskeleton by transporting factors necessary for microtubule integrity to and within the oocyte. These hypotheses are not mutually exclusive and the polarity defects in piRNA pathway mutants may arise from a combination of both mechanisms. Our data support the hypothesis that checkpoint activation leads to more active dynein-mediated transport as reducing the levels of the dynein complex members BicD or dynein partially suppresses the D/V phenotypes of eggs laid by piRNA mutant mothers. BicD is a phosphoprotein and in mammalian cells BicD phosphorylation is necessary for its association with the dynein complex (28). Therefore, it is possible that BicD is itself a target of the Chk-2 checkpoint. Ectopic localization machinery aggregation may thus be driven by a direct modification of the dynein motor machinery.

Finally, dynein-dependent aggregates are associated with many neurodegenerative diseases such as Alzheimer's, Huntington's and amyotrophic lateral sclerosis (ALS) (29, 30). In the mouse model for ALS, overexpression of superoxide dismutase (SOD) leads to SOD aggregation (aggresome-like structures) and lifespan shortening (31, 32). Reducing the levels of dynein activity in the SOD overexpression background suppresses the ALS phenotype, implying that similar cytoskeletal changes to those that we see in our model may occur in these neurodegenerative disorders (33, 34). It will be interesting to see how similar the mechanisms of aggregation are between the 2 systems.

Materials and Methods

***Drosophila* Strains.** All crosses were maintained at 25 °C. The wild-type strain used was Oregon-R. For a list of flies used please see *SI Materials and Methods*. One- to 2-day-old flies were transferred to fresh yeast overnight and then dissected.

Whole-Mount Antibody Staining of Ovaries and in Situ Hybridization. In situ hybridization was performed as described (35). RNA probes were synthesized using the digoxigenin RNA labeling system (Roche). Fast Red detection-based in situ hybridization was done as in ref. 36. Data were gathered using a Zeiss axiophot microscope using an Insight digital camera.

Antibody staining was performed as described (37). For a list of antibodies used please see *SI Materials and Methods*. Data were gathered using a Zeiss 510 LSM confocal microscope. All images were processed using Image J or Photoshop software.

Depolymerization of the Microtubule Network. Flies were fed either yeast paste containing 50 mg/mL colcemid or yeast paste alone for 16–24 h. Ovaries were dissected after this treatment and fixed as described above.

Quantitative RT-PCR. RNA was isolated from ovaries of 2- to 3-day-old fattened females using TRIzol extraction (Invitrogen). RNA was then treated with DNAfree reagent (Ambion) twice to remove contaminating genomic DNA. cDNA was synthesized using 500 ng of RNA and superScript II reverse transcriptase (Invitrogen). One microliter of each reverse transcription reaction was used per real-time reaction, which contained 1× Sybrgreen master mix (ABI) and 0.075 mM gene-specific primers in a 10-μL reaction. Cycling parameters were: 50 °C, 2 min; 95 °C, 10 min; 95 °C, 15 sec; 60 °C, 1 min for 40 cycles in an ABI 7900HT. The following primers were used: HETA: 5′-ATCCTTCACCGTCATCACCTTCCT-3′, 5′-GGTGCGTTTAGGTGAGTGTGTGTT-3′, RP49: 5′-ATGACCATCCGCCCAGCATAC-3′, 5′-CTGCATGAGCAGGACCTCCAG-3′ (10), Adh 5′-CCGTGGTCAACTTCACCAGCTC-3′, 5′-TCCAACCAGGAGTTGAACGTGTGC-3′, mdg1for: 5′-GTCAGAAGGAGGCCATTCAGGAATTT-3′, mdg1rev: 5′-GTTGCTGGCGGTTTCTGTTATTGTCAA-3′ (38). Data were analyzed using SDS software. Statistical significance was calculated using the Student's *t* test.

Western Blotting. Western blotting was done according to Navarro et al. (37). Mouse anti-acetylated-tubulin and mouse anti-β-tubulin (Sigma) were used at 1:10,000. For acetylated tubulin levels in *spnE* mutant ovaries Western blots of 4 independent samples were done. For levels in the *armi* mutant background 3 separate blots representing 3 independent samples were done. For levels in the *aub* mutant background 2 separate blots representing 2 independent samples were done.

Injections. Ovaries from individual flies were dissected in Voltaleff 9S halocarbon oil (VWR) on a 22 × 64-mm coverslip (RA Lamb), with ovarioles teased apart and spread so that they adhered to the glass. Immediately afterward, an RNA injection was performed on an IX71 inverted microscope (Olympus) using a 40×/1.35 NA 340/UApo oil iris objective. Clusters of Egl-RFP were visualized with epifluorescence and the corresponding nurse cells injected with 2-mM solution (in RNase-free water) of Alexa 488–5-UTP-labeled I factor localization element (552 nt, see ref. 4) or Krueppel (full length) mRNA using a fine, heat-pulled glass needle. Images were captured with the Ultraview ERS spinning disk system (Perkin–Elmer) fitted with a Hamamatsu Orca ER CCD camera. Alternate images were taken of fluorescent RNA and Egl-RFP over 15 min, with exposures of 1 sec and 2 sec, respectively. Fluorescent mRNA was produced as described in ref. 39.

ACKNOWLEDGMENTS. We thank members of the Lehmann Lab for their critical reading of this manuscript. We also thank Kenn Albrecht, Vitor Barbosa, Ryan Cinalli, Lilach Gilboa, Prashanth Rangan, and Daria Siekhaus for many helpful discussions and Andy Renault for hanging the RNAi poster. We thank Nadine Schultz (University of Massachusetts, Worcester, MA) for generating the *mnk*,*aub* and *mnk*;*armi* double mutant flies. We thank our colleagues, the Bloomington Drosophila Stock Collection, and the Developmental Studies Hybridoma Bank for antibodies and flies (see *SI Materials and Methods*). R.L. is an investigator of the Howard Hughes Medical Institute.

1. van Eeden F, St Johnston D (1999) The polarisation of the anterior-posterior and dorsal-ventral axes during Drosophila oogenesis. *Curr Opin Genet Dev* 9:396–404.
2. Li M, McGrail M, Serr M, Hays TS (1994) Drosophila cytoplasmic dynein, a microtubule motor that is asymmetrically localized in the oocyte. *J Cell Biol* 126:1475–1494.
3. Vagin VV, et al. (2004) The RNA Interference proteins and vasa locus are involved in the silencing of retrotransposons in the female germline of Drosophila melanogaster. *RNA Biol* 1:54–58.
4. Van De Bor V, Hartswood E, Jones C, Finnegan D, Davis I (2005) gurken and the I factor retrotransposon RNAs share common localization signals and machinery. *Dev Cell* 9:51–62.
5. Cook HA, Koppetsch BS, Wu J, Theurkauf WE (2004) The Drosophila SDE3 homolog armitage is required for oskar mRNA silencing and embryonic axis specification. *Cell* 116:817–829.
6. Gonzalez-Reyes A, Elliott H, St Johnston D (1997) Oocyte determination and the origin of polarity in Drosophila: The role of the spindle genes. *Development* 124:4927–4937.
7. Wilson JE, Connell JE, Macdonald PM (1996) aubergine enhances oskar translation in the Drosophila ovary. *Development* 122:1631–1639.
8. Chen Y, Pane A, Schupbach T (2007) Cutoff and aubergine mutations result in retrotransposon upregulation and checkpoint activation in Drosophila. *Curr Biol* 17:637–642.
9. Klattenhoff C, et al. (2007) Drosophila rasiRNA pathway mutations disrupt embryonic axis specification through activation of an ATR/Chk2 DNA damage response. *Dev Cell* 12:45–55.
10. Pane A, Wehr K, Schupbach T (2007) zucchini and squash encode two putative nucleases required for rasiRNA production in the Drosophila germline. *Dev Cell* 12:851–862.
11. Gillespie DE, Berg CA (1995) Homeless is required for RNA localization in Drosophila oogenesis and encodes a new member of the DE-H family of RNA-dependent ATPases. *Genes Dev* 9:2495–2508.
12. Pare C, Suter B (2000). Subcellular localization of Bic-D::GFP is linked to an asymmetric oocyte nucleus. *J Cell Sci* 113(Pt 12):2119–2127.
13. Styhler S, Nakamura A, Swan A, Suter B, Lasko P (1998) vasa is required for GURKEN accumulation in the oocyte, and is involved in oocyte differentiation and germline cyst development. *Development* 125:1569–1578.
14. Mallik R, Gross SP (2004) Molecular motors: Strategies to get along. *Curr Biol* 14:R971–R982.
15. Theurkauf WE, Alberts BM, Jan YN, Jongens TA (1993) A central role for microtubules in the differentiation of Drosophila oocytes. *Development* 118:1169–1180.
16. Hammond JW, Cai D, Verhey KJ (2008) Tubulin modifications and their cellular functions. *Curr Opin Cell Biol* 20:71–76.
17. Ghabrial A, Ray RP, Schupbach T (1998) okra and spindle-B encode components of the RAD52 DNA repair pathway and affect meiosis and patterning in Drosophila oogenesis. *Genes Dev* 12:2711–2723.
18. Staeva-Vieira E, Yoo S, Lehmann R (2003) An essential role of DmRad51/SpnA in DNA repair and meiotic checkpoint control. *EMBO J* 22:5863–5874.
19. Ghabrial A, Schupbach T (1999) Activation of a meiotic checkpoint regulates translation of Gurken during Drosophila oogenesis. *Nat Cell Biol* 1:354–357.
20. Vagin VV, et al. (2006). A distinct small RNA pathway silences selfish genetic elements in the germline. *Science* 313:305–306.
21. Johnston JA, Illing ME, Kopito RR (2002) Cytoplasmic dynein/dynactin mediates the assembly of aggresomes. *Cell Motil Cytoskeleton* 53:26–38.
22. Johnston JA, Ward CL, Kopito RR (1998) Aggresomes: A cellular response to misfolded proteins. *J Cell Biol* 143:1883–1898.
23. Kwon S, Zhang Y, Matthias P (2007) The deacetylase HDAC6 is a novel critical component of stress granules involved in the stress response. *Genes Dev* 21:3381–3394.
24. Heath CM, Windsor M, Wileman T (2001) Aggresomes resemble sites specialized for virus assembly. *J Cell Biol* 153:449–455.
25. Wileman T (2006) Aggresomes and autophagy generate sites for virus replication. *Science* 312:875–878.
26. Martin SG, Leclerc V, Smith-Litiere K, St Johnston D (2003) The identification of novel genes required for Drosophila anteroposterior axis formation in a germline clone screen using GFP-Staufen. *Development* 130:4201–4215.
27. Steinhauer J, Kalderon D (2006) Microtubule polarity and axis formation in the Drosophila oocyte. *Dev Dyn* 235:1455–1468.
28. Fumoto K, Hoogenraad CC, Kikuchi A (2006) GSK-3beta-regulated interaction of BICD with dynein is involved in microtubule anchorage at centrosome. *EMBO J* 25:5670–5682.
29. Garcia-Mata R, Gao YS, Sztul E (2002) Hassles with taking out the garbage: Aggravating aggresomes. *Traffic* 3:388–396.
30. Kopito RR (2000) Aggresomes, inclusion bodies and protein aggregation. *Trends Cell Biol* 10:524–530.
31. Kieran D, et al. (2005) A mutation in dynein rescues axonal transport defects and extends the life span of ALS mice. *J Cell Biol* 169:561–567.
32. Teuchert M, et al. (2006) A dynein mutation attenuates motor neuron degeneration in SOD1(G93A) mice. *Exp Neurol* 198:271–274.
33. Deng HX, et al. (2006) Conversion to the amyotrophic lateral sclerosis phenotype is associated with intermolecular linked insoluble aggregates of SOD1 in mitochondria. *Proc Natl Acad Sci USA* 103:7142–7147.
34. Jaarsma D, et al. (2000) Human Cu/Zn superoxide dismutase (SOD1) overexpression in mice causes mitochondrial vacuolization, axonal degeneration, and premature motoneuron death and accelerates motoneuron disease in mice expressing a familial amyotrophic lateral sclerosis mutant SOD1. *Neurobiol Dis* 7:623–643.
35. Ephrussi A, Dickinson LK, Lehmann R (1991) Oskar organizes the germ plasm and directs localization of the posterior determinant nanos. *Cell* 66:37–50.
36. Bullock SL, et al. (2004) Differential cytoplasmic mRNA localisation adjusts pair-rule transcription factor activity to cytoarchitecture in dipteran evolution. *Development* 131:4251–4261.
37. Navarro C, Puthalakath H, Adams JM, Strasser A, Lehmann R (2004) Egalitarian binds dynein light chain to establish oocyte polarity and maintain oocyte fate. *Nat Cell Biol* 6:427–435.
38. Aravin AA, et al. (2004) Dissection of a natural RNA silencing process in the Drosophila melanogaster germ line. *Mol Cell Biol* 24:6742–6750.
39. Bullock SL, Nicol A, Gross SP, Zicha D (2006) Guidance of bidirectional motor complexes by mRNA cargoes through control of dynein number and activity. *Curr Biol* 16:1447–1452.